Cross-Correlated Chemical Shift Modulation: A Signature of Slow Internal Motions in Proteins

Dominique Früh,[†] Joel R. Tolman,[†] Geoffrey Bodenhausen,[†,‡] and Catherine Zwahlen*,[†]

Contribution from the Section de Chimie, Université de Lausanne, BCH, 1015 Lausanne, Switzerland, and Département de chimie, associé au CNRS, Ecole Normale Supérieure, 24 rue Lhomond, 75231 Paris cedex 05, France

Received September 25, 2000. Revised Manuscript Received January 30, 2001

Abstract: A novel NMR experiment allows one to characterize slow motion in macromolecules. The method exploits the fact that motions, such as rotation about dihedral angles, induce correlated fluctuations of the isotropic chemical shifts of the nuclei in the vicinity. The relaxation of two-spin coherences involving C^{α} and C^{β} nuclei in proteins provides information about correlated fluctuations of the isotropic chemical shifts of C^{α} and C^{β}. The difference between the relaxation rates of double- and zero-quantum coherences C^{α}_{+} C^{β}_{+} and C^{α}_{+} C^{β}_{-} is shown to be affected by *cross-correlated chemical shift modulation*. In ubiquitin, evidence for slow motion is found in loops or near the ends of β-strands and α-helices.

Introduction

Conformational dynamics and internal mobility play a central role in many biological processes including protein/protein interactions,[1] protein folding,[2] and enzymatic reactions.[3] NMR spectroscopy can in principle provide a vital contribution to the understanding of biomolecules by supplementing structural information through dynamic information. In particular, NMR has a unique ability to assess segmental motions spanning a wide range of time scales. Fast motions on the subnanosecond time scale are usually characterized by a so-called model-free analysis[4] using a combination of longitudinal, transverse, and cross-relaxation rates (T_1, T_2 and nOe). Order parameters are usually measured by using ^{15}N nuclei[5,6] and less frequently by using ^{13}C nuclei.[7] The local order parameter S^2, derived from such an analysis, gives a measure of the amplitude of the fluctuations of a bond vector and thus reflects the local flexibility of a protein. By using appropriate models, such fast scale motions can be described in more detail.[8−10] Slow motions in the microsecond to millisecond range are usually detected by measuring differences between T_2 and $T_{1\rho}$, the latter often recorded as a function of the (possibly tilted) effective RF fields,[11] or using relaxation-compensated CPMG sequences.[12−14] The simplest indication of slow motion is the observation that $T_{1\rho} > T_2$. However, in uniformly ^{13}C-enriched proteins, measuring T_2 and $T_{1\rho}$ for side-chain carbons is fraught with problems, and in practice these methods can only be applied to ^{15}N and carbonyl nuclei, or to proteins that are selectively enriched in particular carbon positions.

In the present paper, we propose a new approach to the study of slow motions through the relaxation rates of multiple quantum coherences. Such motions could be due to the making or breaking of hydrogen bonds, motions of the backbone, large-scale wobbling of a loop, large-amplitude conformational changes of side chains, etc. Such motions, which are expected to occur on a microsecond to millisecond time scale, are much slower than overall tumbling (the rotational correlation times of typical biomolecules being in the range of 3 to 30 ns) so that all anisotropic interactions (dipole−dipole and CSA) have been averaged out by overall tumbling in the protracted intervals between the rare events associated with slow motions. If slow motions are to leave a signature on the NMR response, they must therefore affect *isotropic* properties that are not averaged out by overall tumbling. Indeed, it is known that the making or breaking of a hydrogen bond (N−H···O) modulates not only the orientations and magnitudes of the principal components of the CSA tensors of the nuclei involved but also their isotropic shifts, i.e., the average between the three principal components of the CSA tensor.[15,16] More generally, rotations around dihedral angles affect the isotropic shifts of neighboring nuclei. For example, fluctuations around the dihedral angles ϕ, ψ, and χ_1

* Address correspondence to this author. Phone: +41 21 692 39 86. Fax: +41 21 692 40 35. E-mail: Catherine.Zwahlen@ico.unil.ch.

[†] Université de Lausanne.

[‡] Ecole Normale Supérieure.

(1) Feher, V. A.; Cavanagh, J. *Nature* **1999**, *400*, 289−293.

(2) Eaton, W. A.; Munoz, V.; Hagen, S. J.; Jas, G. S.; Lapidus, L. J.; Henry, E. R.; Hofrichter, J. *Annu. Rev. Biophys. Biomol. Struct.* **2000**, *29*, 327−359.

(3) Radkiewicz, J. L.; Brooks, C. L. *J. Am. Chem. Soc.* **2000**, *122*, 225−231.

(4) Lipari, G.; Szabo, A. *J. Am. Chem. Soc.* **1982**, *104*, 4546−4559.

(5) Peng, J. W.; Wagner, G. *J. Magn. Reson.* **1992**, *98*, 308−332.

(6) Farrow, N. A.; Muhandiram R.; Singer, A. U.; Pascal, S. M.; Kay, C. M.; Shoelson, S. E.; Pawson, T.; Forman-Kay, J. D.; Kay, L. E. *Biochemistry* **1994**, *33*, 5984−6003.

(7) Wand, A. J.; Urbauer, J. L.; McEvoy, R. P.; Bieber R. J. *Biochemistry* **1996**, *35*, 6116−6125.

(8) Daragan, V. A.; Mayo, K. H. *Prog. NMR Spectroc.* **1996**, *31*, 63−105.

(9) Fischer, M. W. F.; Zeng, L.; Pang, Y.; Hu, W.; Majumdar, A.; Zuiderweg, E. R. P. *J. Am. Chem. Soc.* **1997**, *119*, 12629−12642.

(10) Lienin, S. F.; Bremi, T.; Brutscher, B.; Brüschweiler, R.; Ernst, R. R. *J. Am. Chem. Soc.* **1998**, *120*, 9870−9879.

(11) Akke, M.; Palmer, A. G. *J. Am. Chem. Soc.* **1996**, *118*, 911−912.

(12) Ishima, R.; Louis, J. M.; Torchia, D. A. *J. Am. Chem. Soc.* **1999**, *121*, 11589−11590.

(13) Loria, J. P.; Rance, M.; Palmer, A. G. *J. Am. Chem. Soc.* **1999**, *121*, 2331−2332.

(14) Mulder, F. A. A.; Skrynnikov, N. R.; Hon, B.; Dahlquist, F. W.; Kay, L. E. *J. Am. Chem. Soc.* **2001**, *123*, 967−975.

(15) Arnold, W. D.; Oldfield, E. *J. Am. Chem. Soc.* **2000**, *122*, 12835−12841.

(16) Brender, J. R.; Taylor, D. M.; Ramamoorthy, A. *J. Am. Chem. Soc.* **2001**, *123*, 914−922.

10.1021/ja003487k CCC: $20.00
Published on Web 04/26/2001

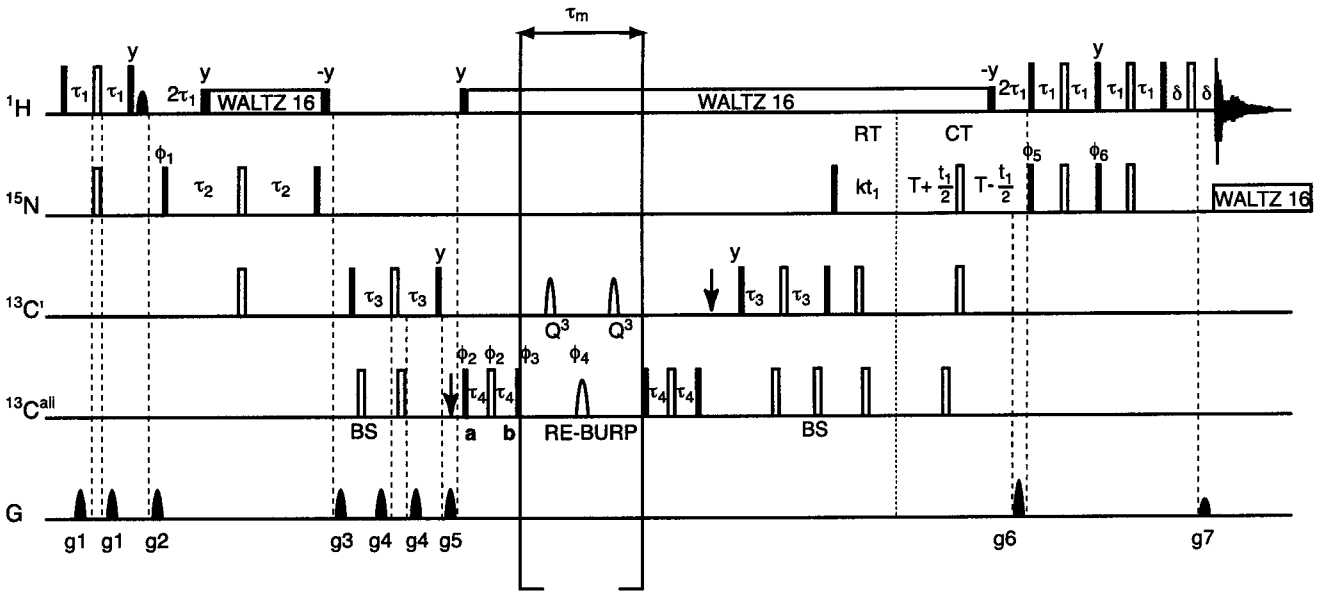

Figure 1. Pulse sequence for the measurement of $C^{\alpha}C^{\beta}$ multiple quantum relaxation. Black and white rectangles indicate $\pi/2$ and π pulses, respectively. The pulses are applied along the *x* axis, unless specified otherwise. The ^{1}H, ^{15}N carriers are positioned at 4.7 and 118 ppm, respectively. The ^{13}C carrier is initially at 175 ppm, then, as indicated by small arrows, moved to 43 ppm prior to the 90° pulse with phase ϕ_2 and back to 175 ppm just before the $90°_y$ pulse applied to $^{13}C'$. Rectangular ^{13}C pulses are applied with field strengths of $\Delta/\sqrt{15}$ and $\Delta/\sqrt{3}$ for 90° and 180° pulses, respectively. When the carrier is positioned at 175 ppm, Δ is defined as the difference in Hz between the centers of the $^{13}C'$ and the $^{13}C^{\alpha}$ regions, while Δ is the difference between the centers of the $^{13}C'$ and the $^{13}C^{ali}$ regions if the carrier is positioned at 43 ppm. Off-resonance pulses applied on $^{13}C^{\alpha}$ (58 ppm) while the carrier is at 175 ppm are phase modulated. Pulses introduced to compensate for Bloch−Siegert phase shifts[53] are labeled with BS. During the mixing time τ_m, the $^{13}C'$ carbons are inverted by two Q^3 pulses[26] of 300 μs. Chemical shift evolution of the multiple quantum coherence is refocused by a 500 μs RE-BURP pulse[23] applied in the middle of τ_m. The delays are set to $\tau_1 = 2.7$ ms ($\approx(4J(NH))^{-1}$), $\tau_2 = 11$ ms ($\approx(4J(C'N))^{-1}$), $\tau_3 = 4.3$ ms ($\approx(4J(C'C^{\alpha}))^{-1}$), $\tau_4 = 7.1$ ms ($\approx(4J(C^{\alpha}C^{\beta}))^{-1}$), and $\delta = 1.3$ ms. The ^{15}N magnetization evolves during a semiconstant time period[27] indicated by RT (real time) and CT (constant time). Quadrature detection in t_1 is obtained by the enhanced-sensitivity pulsed field gradient method[28,29] where for each value of t1 separate data sets are recorded with (g7, ϕ_6) and (−g7, ϕ_6+180°). A water flip-back pulse[31] ensures good water suppression. Proton and nitrogen decoupling are achieved by using the WALTZ-16 sequence[54] with radio frequency field strengths of 7.2 and 1.2 kHz, respectively. The phase cycle is $\phi_1 = x, -x$, $\phi_2 = 4(x), 4(y), 4(-x), 4(-y)$, $\phi_4 = x, y, -x, -y$, $\phi_5 = x, x, -x, -x$, $\phi_6 = y, y, -y, -y$. For selection of zero-quantum coherences, $\phi_3 = 4(x), 4(y), 4(-x), 4(-y), 4(-x), 4(-y), 4(x), 4(y)$ and $\phi_{rec} = 4(x, -x, -x, x), 4(-x, x, x, -x)$; for selection of double-quantum coherences, $\phi_3 = 4(x), 4(y), 4(-x), 4(-y)$ and $\phi_{rec} = 2(x, -x, -x, x, -x, x, x, -x)$. The duration and strengths of the gradients are g1 = (1 ms, 6.5 G/cm), g2 = (1 ms, 46.5 G/cm), g3 = (1 ms, 27 G/cm), g4 = (1 ms, −6.5 G/cm), g5 = (1 ms, −18.5 G/cm), g6 = (1 ms, 40 G/cm), and g7 = (1 ms, 4.05 G/cm).

modulate the isotropic shift of both C^{α} and C^{β} nuclei.[17] The measurement of $T_{1\rho}$ of a nucleus as a function of the effective RF field may be interpreted as a means of ascertaining the amplitude of the fluctuations of the isotropic shift. However, $T_{1\rho}$ studies of single-quantum coherences cannot reveal the details of the dynamic processes.

In this paper, we introduce a new step toward a better characterization of slow conformational exchange. We investigate the transverse relaxation rates of zero-quantum (ZQ) and double-quantum (DQ) coherences of $C^{\alpha}C^{\beta}$ subsystems in isotopicaly enriched proteins. Since rotations around ϕ, ψ, and χ_1 affect the isotropic shifts of both C^{α} and C^{β} nuclei simultaneously, the modulation of these shifts will be correlated. Multiple-quantum spectroscopy is exquisitely sensitive to correlated fluctuations. Thus, the transverse relaxation of a two-spin coherence involving the two spins C^{α} and C^{β} will report not only on the time-dependent fluctuations of the isotropic shifts of the C^{α} and C^{β} sites, as could in principle be obtained from the separate measurement of $T_{1\rho}(C^{\alpha})$ and $T_{1\rho}(C^{\beta})$, but on the extent of correlation of the fluctuations of the isotropic shifts of two sites. We shall use the expression cross-correlated isotropic *c*hemical *s*hift *m*odulation (CSM) to describe this situation. The measurements allow one to distinguish between positive and negative rates corresponding to events generating correlated and anticorrelated CSM, respectively. The pulse sequence presented here allows one to record decay curves of $C^{\alpha}C^{\beta}$ coherences. By fitting these curves, both the effective scalar couplings to the C^{γ} carbons and the auto-relaxation rates of ZQ and DQ coherences can be estimated. The ZQ and DQ coherences have different decay rates since they are sensitive in a different fashion to cross-correlated relaxation mechanisms. A complete analysis of all relaxation pathways is presented, assuming slow isotropic tumbling. In ubiquitin, cross-correlated CSM reveals slow internal motion for several residues located either at the end of secondary structure elements or in loops.

Material and Methods

Uniformly $^{13}C/^{15}N$-enriched ubiquitin was obtained commercially (VLI). The protein was dissolved in 10% D_2O/90% H_2O at pH 4.5 to a concentration of 1.5 mM. NMR data were acquired at 30° C on a Bruker DMX-600 spectrometer equipped with a triple resonance probe with triple axis gradients. 2D spectra were recorded by using the pulse scheme shown in Figure 1 and a data matrix consisting of 64 × 512 complex points was acquired; the spectral widths were 1824 and 8389 Hz in the ω_1 and ω_2 dimensions. A relaxation delay of 1.5 s was employed and 32 scans were accumulated. The total measuring time for a 2D experiment was 1.7 h. The data were processed by using the package NMRPipe/NMRDraw.[18] Each dimension was apodized with a 65° shifted squared sine-bell window function and zero-filled once.

(17) Havlin, R. H.; Le, H.; Laws, D. D.; deDios, A. C.; Oldfield, E. *J. Am. Chem. Soc.* **1997**, *119*, 11951−11958.

(18) Delaglio, F.; Grzesiek, S.; Vuister, G. W.; Zhu, G.; Pfeifer, J.; Bax, A. *J. Biomol. NMR* **1995**, *6*, 277−293.

Relaxation rates and scalar coupling constants were obtained by least-squares fitting of the decay curves, implemented by using the Levenberg−Marquart algorithm in Matlab.[19] Errors were estimated by using a Monte Carlo analysis with 300 synthetic data sets.[20]

Results and Discussion

Pulse Sequence. The pulse sequence designed for measuring decay rates of $C^{\alpha}C^{\beta}$ zero- and double-quantum coherences is shown in Figure 1. During the preparation period, amide proton magnetization is transferred from H^N to C^{α} in a HNCOCA fashion[21] leading to a doubly antiphase single-quantum coherence $4C_y^{\alpha}N_zC'_z$ (**a**) that is converted into $8C_x^{\alpha}C_z^{\beta}N_zC'_z$ at point **b** following evolution under the one-bond scalar coupling $^1J(C^{\alpha}C^{\beta})$. A $90°_x$ pulse applied to the aliphatic carbons creates the desired ZQ and DQ coherences which can be separated by phase cycling of the three pulses prior to the relaxation period.[22] The ZQ (respectively DQ) coherences correspond to density operator elements of the form $4C_+^{\alpha}\,C_-^{\beta}\,N_zC'_z - 4C_-^{\alpha}\,C_+^{\beta}\,N_zC'_z$ (respectively $4C_+^{\alpha}\,C_+^{\beta}\,N_zC'_z - 4C_-^{\alpha}\,C_-^{\beta}N_zC'_z$), that have relaxation properties similar to $C_+^{\alpha}\,C_-^{\beta} - C_-^{\alpha}\,C_+^{\beta}$ (respectively $C_+^{\alpha}\,C_+^{\beta} - C_-^{\alpha}\,C_-^{\beta}$) in the slow tumbling limit. Gradient selection would result in a loss of a factor of 2 in sensitivity for the DQ coherence, since only the P- or N-type pathway could be selected. During the relaxation period τ_m, relaxation of the ZQ and DQ coherences is monitored, while chemical shift evolution is refocused by a RE-BURP pulse[23] covering the aliphatic region. As a result, scalar couplings between aliphatic C^{γ} carbons and the ZQ or DQ coherences are not averaged and cause a cosine modulation of the decaying coherences. Proton decoupling prevents the conversion from in-phase into antiphase magnetization through the evolution of the one-bond $^1H-^{13}C$ scalar couplings that would complicate the analysis of the decay curves.[24,25] Cross-correlated mechanisms involving either the $C^{\alpha}C'$ or the $C^{\beta}C'$ dipoles are averaged out by the two Q^3 pulses[26] applied to the carbonyl C′ nuclei. At the end of the relaxation period, the magnetization is transferred back to H^N. To optimize resolution and sensitivity, $^1H-^{15}N$ correlation is achieved by labeling the signal in a semiconstant time manner[27] using the sensitivity enhancement technique[28,29] in the final transfer step. Two *z*-filters are inserted during the preparation period to eliminate unwanted coherences.[30] The use of a water flip-back pulse[31] in concert with gradient selection provides good water suppression.

$C^{\alpha}C^{\beta}$ Relaxation. The relaxation of $C^{\alpha}C^{\beta}$ ZQ and DQ coherences arises from a combination of auto- and cross-correlated mechanisms. Figure 2 shows the cross-correlated mechanisms that are not averaged out during the relaxation period τ_m. The relaxation modes depicted in Figure 2a−d cause differential line broadening, i.e., a difference between zero- and double-quantum relaxation rates. The three cross-correlation mechanisms shown in Figure 2a−c contribute to the auto-relaxation of the multiple quantum coherences, while those of Figure 2d,e cause cross-relaxation leading to the build-up of doubly antiphase terms such as $4C_+^{\alpha}\,C_+^{\beta}\,H_z^{\alpha}\,H_z^{\beta}$, a process which is accompanied by a multiexponential decay of the multiple quantum coherences. However, for short mixing times the relaxation of $C^{\alpha}C^{\beta}$ ZQ and DQ coherences can be considered to be monoexponential:

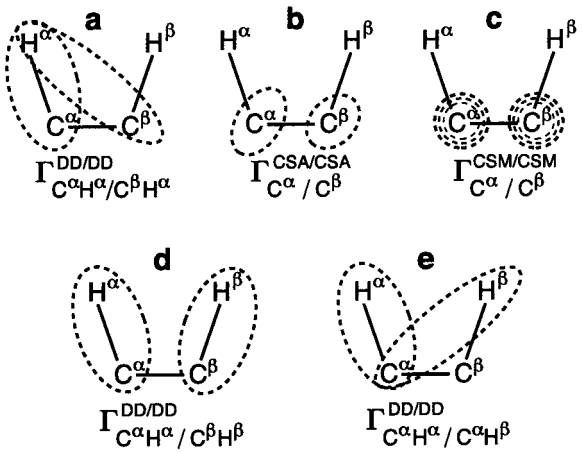

Figure 2. Selected cross-correlated mechanisms that affect the relaxation of $C^{\alpha}C^{\beta}$ multiple quantum coherences. (a−c) Cross-correlated effects that contribute to auto-relaxation. (a) Dipole/dipole cross-correlation involving a single external spin (here H^{α}), (b) CSA/CSA cross-correlation, and (c) correlated isotropic chemical shift modulations (CSM). These mechanisms induce differential line broadening when comparing the ZQ and DQ line widths. (d−e) Cross-correlated relaxation mechanisms that may transform the initial coherence $C_+^{\alpha}\,C_+^{\beta}$ or $C_+^{\alpha}\,C_-^{\beta}$ into doubly antiphase terms with respect to H^{α} and H^{β}, i.e. $4C_+^{\alpha}\,C_+^{\beta}H_z^{\alpha}\,H_z^{\beta}$ or $4C_+^{\alpha}\,C_-^{\beta}H_z^{\alpha}\,H_z^{\beta}$. The mechanism shown in (d) gives rise to differential relaxation of ZQ vs DQ coherences, while the contributions depicted in (e) have the same effect on both coherences. For the mechanisms (a), (d), and (e) all permutations of the C^{α}, C^{β} and H^{α}, H^{β} nuclei must be considered. Depending on the amino acid, mechanisms involving $H^{\beta 1}$, $H^{\beta 2}$, or $H^{\beta 3}$ will also affect $C^{\alpha}C^{\beta}$ relaxation.

$$\langle C_+^{\alpha}\,C_-^{\beta}\,\rangle(\tau_m) = \exp\{-\Gamma^{AR}(ZQ)\tau_m\}\langle C_+^{\alpha}\,C_-^{\beta}\,\rangle(0) \quad (1a)$$

$$\langle C_+^{\alpha}\,C_+^{\beta}\,\rangle(\tau_m) = \exp\{-\Gamma^{AR}(DQ)\,\tau_m\}\langle C_+^{\alpha}\,C_+^{\beta}\,\rangle(0) \quad (1b)$$

and likewise for the complex conjugates. The auto-relaxation rate Γ^{AR} arises from a linear combination of auto-correlated rates $\Gamma^{AR(AC)}$ and cross-correlated rates $\Gamma^{AR(CC)}$. In the slow tumbling limit, the auto-correlated relaxation rates $\Gamma^{AR(AC)}(ZQ)$ of ZQ coherence and $\Gamma^{AR(AC)}(DQ)$ of DQ coherence differ only by the relaxation induced by the $C^{\alpha}C^{\beta}$ dipole:[32]

$$\Gamma^{AR(AC)}(DQ) - \Gamma^{AR(AC)}(ZQ) = \frac{1}{10}\left(\frac{\mu_0}{4\pi}\right)^2 \frac{\hbar^2\,\gamma_C^4}{r_{C\alpha C\beta}^6}\,\tau_c \quad (2)$$

where μ_0 is the permittivity constant in vacuum, γ the gyromagnetic ratio, and τ_c the correlation time of the protein. For a molecule like ubiquitin at 30 °C, with $\tau_c = 4.1$ ns,[33] this difference is negligible (<0.07 Hz), hence $\Gamma^{AR(AC)}(ZQ) \approx$

(19) *Matlab Reference Guide*; Matlab: Natick, MA, 1992.
(20) Bevington, P. R.; Robinson, D. K. *Data Reduction and Error Analysis for the Physical Sciences*, 1992; McGraw-Hill, 2nd Ed.
(21) Kay, L. E.; Ikura, M.; Tschudin, R.; Bax, A. *J. Magn. Reson.* **1990**, *89*, 496−514.
(22) Wokaun, A.; Ernst, R. R. *Chem. Phys. Lett.* **1977**, *52*, 407−412.
(23) Geen, H.; Freeman, R. *J. Magn. Reson.* **1991**, *93*, 93−141.
(24) Vold, R. R.; Vold, R. L. *J. Chem. Phys.* **1976**, *64*, 320−332.
(25) Palmer, A. G.; Skelton, N. J.; Chazin, W. J.; Wright, P. E.; Rance, M. *Mol. Phys.* **1992**, *75*, 699−711.
(26) Emsley, L.; Bodenhausen, G. *J. Magn. Reson.* **1992**, *97*, 135−148.
(27) (a) Logan, T. M.; Olejniczak, E. T.; Xu, R. X.; Fesik, S. W. *J. Biomol. NMR* **1993**, *3*, 225. (b) Grzesiek, S.; Bax, A. *J. Biomol. NMR* **1993**, *3*, 185−204.
(28) Palmer, A. G.; Cavanagh, J.; Wright, P. E.; Rance, M. *J. Magn. Reson.* **1991**, *93*, 151−170.
(29) Kay, L. E.; Keifer, P.; Saarinen, T. *J. Am. Chem. Soc.* **1992**, *114*, 10663−10665.
(30) Sørensen, O. W.; Rance, M.; Ernst, R. R. *J. Magn. Reson.* **1984**, *56*, 527−534.
(31) Grzesiek, S.; Bax, A. *J. Am. Chem. Soc.* **1993**, *115*, 12593−12594.
(32) Macura, S.; Huang, Y.; Suter, D.; Ernst, R. R. *J. Magn. Reson.* **1981**, *43*, 259−281.

$\Gamma^{AR(AC)}(DQ) \approx \Gamma^{AR(AC)}$. Our analysis of cross-correlated rates therefore focuses on the three mechanisms shown in Figure 2a−c, which lead to relaxation rates that contribute with opposite signs for ZQ and DQ coherences. As a result, their respective auto-relaxation rates can be expressed as:

$$\Gamma^{AR}(ZQ) = \Gamma^{AR(AC)} - \Gamma^{AR(CC)} \tag{3a}$$

$$\Gamma^{AR}(DQ) = \Gamma^{AR(AC)} + \Gamma^{AR(CC)} \tag{3b}$$

Clearly the difference $\Delta\Gamma^{AR} = \Gamma^{AR}(DQ) - \Gamma^{AR}(ZQ) = 2\Gamma^{AR(CC)}$ depends only on cross-correlated mechanisms. For a rigid molecule, dipole/dipole and CSA/CSA cross-correlation (Figure 2a,b) fully account for $\Delta\Gamma^{AR}$. However, conformational mobility or chemical exchange may cause fluctuations of the *isotropic* chemical shifts, which may also contribute to relaxation.[34] For two spins, chemical shift modulation can be described by the following Hamiltonian:

$$H(t) = \delta\omega_\alpha(t)C_z^\alpha + \delta\omega_\beta(t)C_z^\beta \tag{4}$$

where $\delta\omega_{\alpha,\beta}(t)$ are the time-dependent deviations from the average isotropic shifts defined so that $\langle\delta\omega_{\alpha,\beta}(t)\rangle = 0$. In the case of ZQ and DQ coherences, CSM induces relaxation through both auto- and cross-correlated mechanisms. The CSM/CSM cross-correlation rate ($\Gamma^{CSM/CSM}_{C^\alpha/C^\beta}$) can be calculated by using Redfield theory:

$$\Gamma^{CSM/CSM}_{C^\alpha/C^\beta}(C_i^\alpha C_j^\beta) = \frac{1}{2}\frac{\langle C_i^\alpha C_j^\beta[C_z^\alpha,[C_z^\beta,C_i^\alpha C_j^\beta]]\rangle}{\langle C_i^\alpha C_j^\beta|C_i^\alpha C_j^\beta\rangle} J^{CSM}_{\alpha\beta}(0) \tag{5}$$

where i and $j = +$ or $-$. Note that because of the form of the Hamiltonian of eq 4, the only relevant component of the spectral density is at zero frequency, regardless of the correlation time τ_c of rotational diffusion. The cross-correlation spectral density for CSM is:

$$J^{CSM}_{\alpha\beta}(0) = \int_{-\infty}^{\infty} \overline{\delta\omega_\alpha(t)\delta\omega_\beta(t-\tau)}\, d\tau \tag{6}$$

Relaxation rates derived from eq 5 have opposite signs for DQ and ZQ coherences, leading to differential line broadening.[35−37] Thus the difference between the relaxation rates of the DQ and ZQ coherences is equal to:

$$\Delta\Gamma^{AR} = 2\sum_i \Gamma^{DD/DD}_{C\alpha Hi/C\beta Hi} + 2\Gamma^{CSA/CSA}_{C^\alpha/C^\beta} + 2\Gamma^{CSM/CSM}_{C^\alpha/C^\beta} \tag{7}$$

where the summation runs over all external spins $i = \alpha, \beta_1, \beta_2, \beta_3$. In the slow isotropic tumbling regime with fast internal motions[38] and for axially symmetric CSA tensors, the terms in eq 7 can be rewritten as:[39, 40]

$$\sum_i \Gamma^{DD/DD}_{C\alpha Hi/C\beta Hi} = \frac{1}{2}\sum_i d_{C\alpha Hi}d_{C\beta Hi}\frac{1}{3}J^{DD/DD}(0)\frac{1}{2}(3\cos^2(\theta_{\alpha i,\beta i}) - 1) \tag{8a}$$

$$\Gamma^{CSA/CSA}_{C^\alpha/C^\beta} = \frac{1}{2}c_{C\alpha}c_{C\beta}\frac{4}{3}J^{CSA/CSA}(0)\frac{1}{2}(3\cos^2(\theta_{\alpha,\beta}) - 1) \tag{8b}$$

where $\theta_{\alpha i,\beta i}$ denotes the angle subtended by the $C^\alpha H^i$ and $C^\beta H^i$ vectors and $\theta_{\alpha,\beta}$ the angle between the symmetry axes of the two CSA tensors. The dipolar and chemical shift anisotropy interaction constants are given by:[41]

$$d_{CiHi} = \sqrt{6}\frac{\mu_0}{4\pi}\cdot\hbar\cdot\frac{\gamma_C\gamma_H}{r^3_{CiHi}} \tag{9a}$$

$$c_{Ci} = \sqrt{\frac{2}{3}}\Delta\sigma_{Ci}\gamma_C B_0 \tag{9b}$$

where $\Delta\sigma_{Cj}$ is the chemical shift anisotropy, B_0 the static magnetic field, and $j = \alpha, \beta$. For fast internal motions the auto-correlation spectral density is given by:[4]

$$J^{DD/DD}(0) = \frac{2\tau_c}{5}S^2_{DD/DD} \tag{10a}$$

$$J^{CSA/CSA}(0) = \frac{2\tau_c}{5}S^2_{CSA/CSA} \tag{10b}$$

where τ_c is the correlation time of the protein and S^2 are the generalized order parameters.

Only the last term in eq 7 is relevant in this study. Although CSA/CSA cross-correlation (eq 8b) is sensitive to conformational mobility in that it reflects the average rate over all conformations, it tends to be negligible (even at 14 T) since the anisotropies of C^α and C^β shift tensors are quite small. Using the experimental observations of Fu et al.[42] and of Bax et al.,[43] we can estimate that $\Delta\sigma_{max}(C^\alpha) = 43$ ppm and $\Delta\sigma_{max}(C^\beta) = 45$ ppm. In the worst possible case, assuming two axially symmetric tensors with unique axes that are parallel, we can estimate that CSA/CSA cross-correlation may contribute about 0.16 s^{-1} for $\tau_c = 4.1$ ns in ubiquitin. The dipole/dipole cross-correlation rates in eq 8a can be calculated (see below) and are invariant to conformational mobility, since the angles $\theta_{\alpha i,\beta i}$ are independent of the torsion angles χ_1, ψ, and ϕ.

In summary, the contribution of cross-correlated CSM can be obtained from the difference between the experimental rates after subtracting the calculated dipole/dipole cross-correlation rate:

$$\Gamma^{CSM/CSM}_{C^\alpha/C^\beta} = \frac{1}{2}\Delta\Gamma^{AR} - \sum_i \Gamma^{DD/DD}_{C\alpha Hi/C\beta Hi} \tag{11}$$

If one has a completely deuterated protein, the magnitude of the dipolar term in eq 11 is attenuated by $(\gamma_H/\gamma_D)^2$, i.e., by a factor of about 42.

Determination of Scalar Couplings and Relaxation Rates. Using the pulse sequence described in Figure 1, we measured the decay of $C^\alpha C^\beta$ ZQ and DQ coherences by varying the relaxation time τ_m between 1 and 60 ms. Since scalar couplings

(33) Schneider, D. M.; Dellwo, M. J.; Wand, A. J. *Biochemistry* **1992**, *31*, 3645−3652.
(34) Deverell, C.; Morgan, R. E.; Strange, J. H. *Mol. Phys.* **1970**, *18*, 553−559.
(35) Wokaun, A.; Ernst, R. R. *Mol. Phys.* **1978**, *36*, 317−341.
(36) Konrat, R.; Sterk, H. *Chem. Phys. Lett.* **1993**, *203*, 75−80.
(37) Tessari, M.; Vuister, G. W. *J. Biomol. NMR* **2000**, *16*, 171−174.
(38) Tjandra, N.; Szabo, A.; Bax, A. *J. Am. Chem. Soc.* **1996**, *118*, 6986−6991.
(39) Boyd, J.; Hommel, U.; Krishnan, V. V. *Chem. Phys. Lett.* **1991**, *187*, 317−324.
(40) Norwood, T. J.; Tillett, M. L.; Lian, L.-Y. *Chem. Phys. Lett.* **1999**, *300*, 429−434.
(41) Cavanagh, J.; Fairbrother, W. J.; Palmer, A. G.; Skelton, N. J. *Protein NMR Spectroscopy Principles and Practice*; Academic Press: San Diego, 1996.
(42) Ye, C.; Fu, R.; Hu, J.; Hou, L.; Ding, S. *Magn. Reson. Chem.* **1993**, *31*, 699−704.
(43) Tjandra, N.; Bax, A. *J. Am. Chem. Soc.* **1997**, *119*, 9576−9577.

to aliphatic C^γ carbons are not refocused during τ_m, the decay curves are modulated by the evolution of the effective scalar couplings $J_{eff}^{ZQ} = |^1J(C^\beta C^\gamma) - {}^2J(C^\alpha C^\gamma)|$ for ZQ and $J_{eff}^{DQ} = |^1J(C^\beta C^\gamma) + {}^2J(C^\alpha C^\gamma)|$ for DQ coherences. Amino acid residues are separated into three categories according to their topology: no aliphatic C^γ carbons (e.g. Ala, Ser, Phe, Tyr, Asn, ...), one aliphatic C^γ atom (Leu, Thr, Gln, ...), and two aliphatic C^γ atoms (Val, Ile). In Figure 3a−c, a few typical decay curves are shown with their respective Fourier transforms for the three types of residues. Fitting the decay curves up to 60 ms with an exponential decay multiplied by $[\cos(\pi J_{eff}\,\tau_m)]^n$, where n is the number of aliphatic C^γ carbons, allows one to extract the effective scalar couplings, which are on average 35 ± 1 Hz for ZQ coherences and 33 ± 1 Hz for DQ coherences. Further work is in progress to improve the accuracy of the measurements.[44] Moreover, the sum of the two effective couplings $^1/_2(J_{eff}^{ZQ} + J_{eff}^{DQ})$ gives the one-bond scalar coupling $^1J(C^\beta C^\gamma)$, while the two-bond $^2J(C^\alpha C^\gamma)$ coupling is obtained from the difference $^1/_2(J_{eff}^{DQ} - J_{eff}^{ZQ})$ (see Supporting Information, Table 2).

Since cross-correlation mechanisms shown in Figure 2d,e are not suppressed by proton decoupling and not averaged out during the relaxation period, the multiexponential character of the decays becomes important at long mixing times. To a good approximation, however, the decays are monoexponential for $\tau_m < 30$ ms (eq 1) with a characteristic auto-relaxation rate Γ^{AR} defined in eq 3. The decay rates were obtained by fitting each curve for $1 < \tau_m < 30$ ms with an exponential function multiplied by $[\cos(\pi J_{eff}\,\tau_m)]^n$, where n is the number of aliphatic C^γ carbons and J_{eff} is the coupling constant obtained by fitting the data up to 60 ms. Decay curves of ZQ and DQ coherences for two glutamic acid residues are shown in Figure 3d,e. For E24 the difference $\Delta\Gamma^{AR}$ in relaxation rates between DQ and ZQ coherences is small (Figure 3d), while for E34 (Figure 3e) $\Delta\Gamma^{AR}$ is larger than expected from dipole/dipole cross-correlation alone. This indicates that residue 34 is undergoing conformational exchange.

Out of the 64 detectable residues, 6 were disregarded because of overlapping signals, corresponding to V17, V26, I30, H68, L71, and R72. Visual inspection of the curves showed that differences in the relaxation rates of DQ and ZQ coherences of residues with two C^γ atoms (I3, V5, I13, V17, I23, V26, I30, I36, I44, I61, V70) are masked by the cosine-squared modulation. These residues were therefore removed from the final analysis. Since the primary focus is to detect residues that present deviations between measured relaxation rates and those predicted from eq 8a, an additional 16 residues were excluded on the basis of large χ^2 values during the fitting procedure or large errors in the Monte Carlo analysis, namely M1, L15, E16, P19, D21, N25, A28, Q41, R42, A46, E51, S57, Y59, N60, S65, and T66. Moreover, the values of J_{eff}^{ZQ} and J_{eff}^{DQ} were varied systematically, within 5 Hz of the fitted values, to check that unusual $\Delta\Gamma^{AR}$ were not a mere side-effect of fitting errors. In the end, 36 residues uniformly distributed along the primary sequence were retained for the analysis. Differences in decay rates $\Delta\Gamma^{AR}$ are shown in Figure 4. They range from 1.6 to 13.7 s^{-1} with an average value of 7.4 s^{-1}.

Cross-Correlated CSM. The relaxation rates of $C^\alpha C^\beta$ ZQ and DQ coherences were measured by using the pulse sequence of Figure 1. It was shown that in the initial rate regime, when the relaxation mechanisms shown in Figure 2d,e can be neglected, the difference $\Delta\Gamma^{AR}$ depends only on the three cross-correlated mechanisms shown in Figure 2a,c. For a rigid residue, dipole/dipole cross-correlation $C^\alpha H^i/C^\beta H^i$ (with $i = \alpha, \beta$, see Figure 2a) is the main source of differential line broadening. For ubiquitin, these rates were estimated by means of eq 8a using the X-ray structure[45] to take into account variations in local geometry. Note that the angle $\theta_{\alpha i,\beta i}$ subtended by the two dipoles is invariant to rotations around the dihedral angle χ_1, so that the calculated cross-correlation rate $\Gamma^{DD/DD}_{C^\alpha H^i/C^\beta H^i}$ reflects only the *number* of β-protons. For a correlation time $\tau_c = 4.1$ ns, the dipolar term of eq 8a ranges approximately from 5.6, 8.4, and 12.0 s^{-1} for residues with one, two, or three β-protons, respectively. These rates would drop to approximately 0.1, 0.2, and 0.3 s^{-1} if the protein was deuterated.

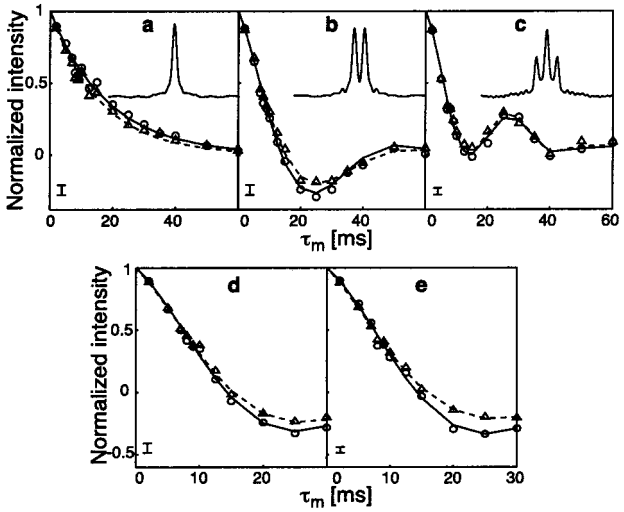

Figure 3. Examples of decay curves for amino acids with none, one, or two aliphatic C^γ carbon atoms. ZQ decays correspond to circles and solid lines, while DQ decays are represented by triangles and dashed lines. (a−c) Relaxation curves with their Fourier transforms. (a) Since the C^γ magnetization of D58 is not inverted by the refocusing pulse in the relaxation period, $^1J(C^\beta C^\gamma)$ is effectively decoupled leading to a singlet after Fourier transform of the decay curve. (b) For L67, the decay curves are modulated by effective couplings to the C^γ nucleus, giving rise to a doublet in the frequency domain. (c) For V5, the Fourier transform of the decay curve gives a degenerate doublet-of-doublets since the effective couplings to the two C^γ carbons are identical. (d−e) Initial rate domain used to obtain auto-relaxation rates. (d) For E24, the difference of the auto-relaxation rates of the ZQ and DQ coherences agrees with the rate predicted by dipole/dipole cross-correlation alone. (e) E34 exhibits a larger difference between the two decay rates that can be attributed to cross-correlated chemical shift modulation (CSM). The average error on peak integration is shown in the lower left corner of each graph.

Dynamic effects cause deviations from these predictions which are based on the assumption of a rigid molecule. Fast internal motions in the picosecond to nanosecond time scale lead to a decrease of the order parameter S^2. For the $\Gamma^{DD/DD}_{C^\alpha H^\alpha/C^\beta H^\alpha}$ cross-correlation rate, we assumed variations of S^2 to be similar to those described for the NH^N/NH^N auto-correlation interaction, namely $0.7 < S^2 < 1$.[10] For the rate $\Gamma^{DD/DD}_{C^\alpha H^{\beta i}/C^\beta H^{\beta i}}$, we used $0.4 < S^2 < 1$, corresponding to the range of order parameters of the $C^\beta D^{\beta i}/C^\beta D^{\beta i}$ auto-correlation interaction.[46] Differences that can be accounted for in this manner by fast local dynamics are represented by the gray zone in Figure 4. Clearly, most differences between predicted and experimental $\Delta\Gamma^{AR}$ can be thus explained by fast motions on the picosecond to nanosecond time scale. However, residues marked by filled diamonds in

(44) Früh, D.; Quebatt, L.; Zwahlen, C.; Bodenhausen, G. In preparation.

(45) Vijay-Kumar, S.; Bugg, C. E.; Cook, C. J. *J. Mol. Biol.* **1987**, *194*, 531−544.

(46) Yang, D.; Mittermaier, A.; Mok, Y.-K.; Kay, L. E. *J. Mol. Biol.* **1998**, *276*, 939−954.

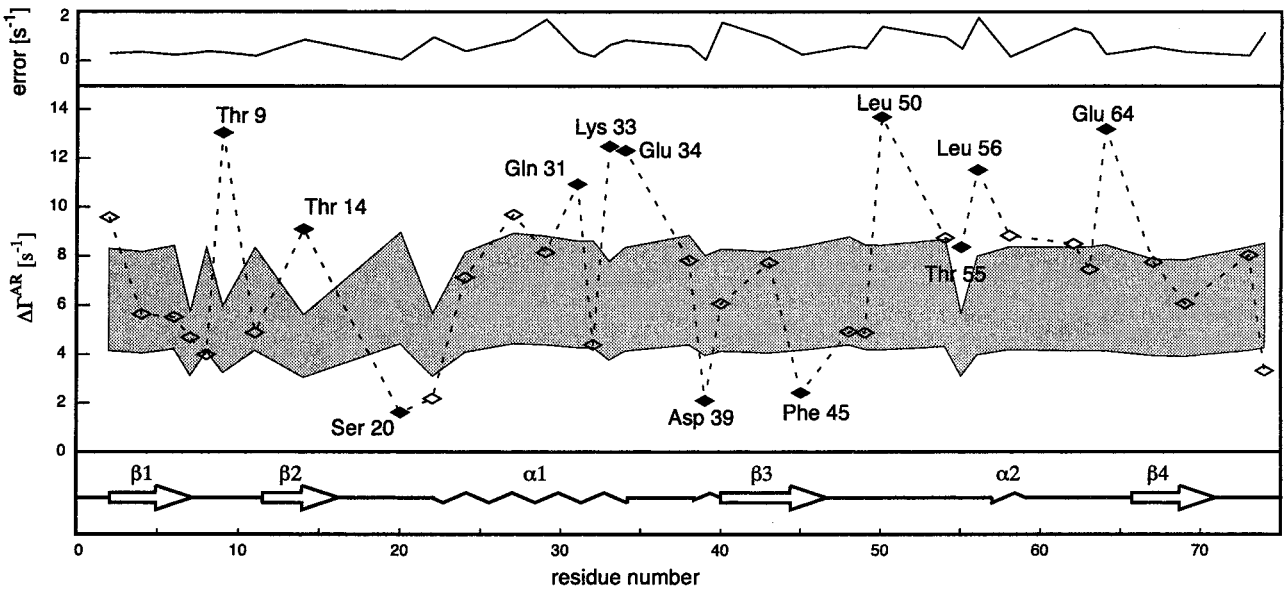

Figure 4. Difference between DQ and ZQ autorelaxation rates. Diamonds correspond to experimental results. The shaded area represents the range that can be explained by dipole/dipole cross-correlated mechanisms (see text for more details). The upper bound corresponds to rates estimated with $S^2 = 1.0$, while the lower bound was calculated by using $S^2 = 0.7$ for dipole/dipole cross-correlations involving H^α and $S^2 = 0.4$ for those involving H^β. Filled diamonds indicate residues that exhibit cross-correlated CSM. Errors estimated by Monte Carlo analysis are shown in the upper part of the figure. The secondary structure of ubiquitin is displayed in the lower part. Arrows indicate β-strands, zigzag lines α-helical domains, and solid lines random coils.

Figure 4 exhibit rates that cannot be explained by reasonable variations of the order parameters. These discrepancies must be due to cross-correlated CSM as depicted in Figure 2c. Since correlated modulations of the isotropic shifts of two carbon atoms are not affected by overall tumbling, cross-correlated CSM is a sensitive probe for motions on the microsecond to millisecond time scale. Various dynamic processes may lead to cross-correlated chemical shift modulation, such as rotations around dihedral angles (ψ, ϕ, χ_1, etc.), slow collective motions, fluctuations of intramolecular interactions, transient hydrogen bonds, exchange with solvent molecules, etc.

In ubiquitin, most of the 12 residues identified as undergoing slow exchange are located in loops or near the ends of secondary structure elements, regions which are usually assumed to feature higher mobility. For the residues shown in Figure 5, rotations around various dihedral angles would be most likely to occur, thus modulating the chemical shifts of both C^α and C^β nuclei. Indeed it is well known that the isotropic C^α and C^β chemical shifts depend on secondary structure[47,48] and that C^α nuclei are deshielded when going from helical to extended conformations, while C^β nuclei are shielded. Rotations around χ_1 can lead to all possible combinations of up- and downfield shifts of the C^α and C^β chemical shifts.[17] Dihedral angle rotations can therefore give rise to either correlated or anti-correlated modulations of the chemical shifts of the two nuclei and hence can lead to positive or negative cross-correlated CSM rates.

Indeed both cases are observed in the present work. S20, D39, and F45 are residues subject to anticorrelated fluctuations of the isotropic shifts of C^α and C^β, while the rates of T9, T14, Q31, K33, E34, L50, T55, L56, and E64 show a positive correlation. Clearly a more detailed interpretation of these results would require a deeper knowledge of the effects of the motions described above on the isotropic shifts of the C^α and C^β carbons for each residue. In principle, further experimental information could be obtained by using $T_{1\rho}$ or CPMG techniques applied to

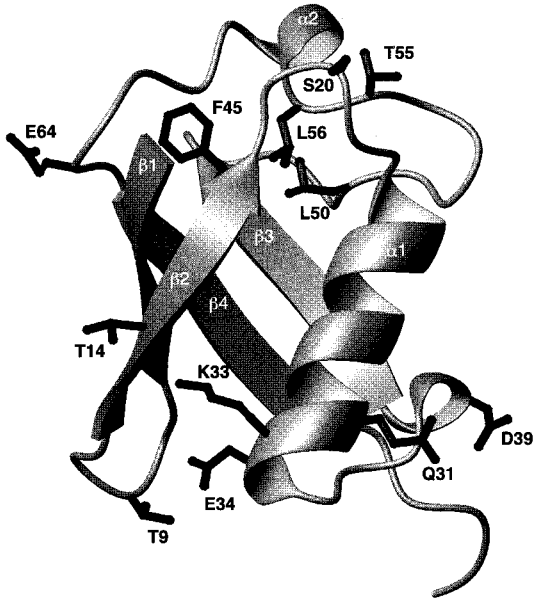

Figure 5. Ribbon representation of an X-ray structure of ubiquitin (1ubq.pdb[45]). Side chains are shown for all residues where cross-correlated CSM has been observed. The figure was made with the program MOLMOL.[55]

C^α and C^β single-quantum coherences to determine their auto-correlated CSM rates. Unfortunately, for a fully ^{13}C-enriched protein, as it is most frequently encountered, both techniques will suffer from complications arising from scalar coupling.

Interestingly, residues Q31, K33, and E34, which are located near the C-terminus of the first α1 helix, all reveal significant cross-correlated CSM. Recently, a detailed analysis of various cross-correlation rates suggested that slow cooperative motions of that helix might occur.[49] Case et al. have shown that averaging of scalar couplings in ubiquitin could only be explained by slow

(47) Spera, S.; Bax, A. *J. Am. Chem. Soc.* **1991**, *113*, 5490−5492.
(48) Wishart, D. S.; Sykes, B. D. *Methods Enzymol.* **1994**, *239*, 363−392.
(49) Carlomagno, T.; Maurer, M.; Hennig, M.; Griesinger, C. *J. Am. Chem. Soc.* **2000**, *122*, 5105−5113.

time scale conformational fluctuations.[50] A quantitative interpretation of cross-correlated chemical shift modulation would require a rigorous treatment based on ab initio chemical shift tensor calculations to establish a relationship between CSM and rotations around dihedral angles. Such an analysis could be very powerful, but is beyond the scope of the present work.

Conclusions

We have presented a new experiment designed to study slow motions in biomolecules. The differences of the relaxation rates of ZQ and DQ coherences involving C^{α} and C^{β} nuclei depends, inter alea, on the correlated fluctuations of the isotropic shifts of C^{α} and C^{β} nuclei that arises from slow internal rotations. In ubiquitin our method revealed the presence of both correlated and anticorrelated chemical shift modulation of these nuclei.

The relaxation behavior of other pairs of nuclei can be readily studied by using the methodology described in this paper. The combination of multiple relaxation rates derived from different nuclei would provide a unique tool to characterize slow motions in macromolecules. In a recent contribution by Kloiber and Konrat, cross-correlated chemical shift modulation has been shown to affect relaxation in $H^{N}N$ systems.[51] Other manifestations of cross-correlated CSM have been observed for $^{15}N-$ ^{15}N ZQ and DQ coherences in nucleic acids.[52] Clearly, cross-correlated chemical shift modulation promises to extend our ability to observe and characterize motions on slow time scales.

Acknowledgment. We thank Dr. Sébastien Vincent for critical reading of the manuscript, Dr. Robert Konrat for a preprint of his work, and Dr. Elisabetta Chiarparin for many stimulating discussions. The research was supported by the Fonds National de la Recherche Scientifique (C.Z. No. 31-56951.99) and by the Commission pour la Technologie et l'Innovation (G.B.).

Supporting Information Available: Spectra obtained with the pulse sequence of Figure 1 and two tables containing the measured and calculated rates $\Delta\Gamma^{AR}$, as well as the effective scalar couplings J_{eff}^{ZQ} and J_{eff}^{DQ}, and the couplings $^{1}J(C^{\alpha}C^{\beta})$ and $^{2}J(C^{\alpha}C^{\gamma})$ (PDF). This material is available free of charge via the Internet at http://pubs.acs.org.

JA003487K

(50) Case, D. A.; Scheurer, C.; Brüschweiler, R. *J. Am. Chem. Soc.* **2000**, *122*, 10390−10397.

(51) Kloiber, K.; Konrat, R. *J. Biomol. NMR* **2000**, *18*, 33−42

(52) Chiarparin, E.; Rüdisser, S.; Bodenhausen, G. *Chem. Phys. Chem.* **2001**, *1*, 41−45.

(53) Emsley, L.; Bodenhausen, G. *Chem. Phys. Lett.* **1990**, *168*, 297−303.

(54) Shaka, A. J.; Keeler, J.; Frenkiel, T.; Freeman, R. *J. Magn. Reson.* **1983**, *52*, 335.

(55) Koradi, R.; Billeter, M.; Wütrich, K. *J. Mol. Graphics* **1996**, *14*, 51−55.